

CO in HI Self-Absorbed Clouds in Perseus

P. D. Klaassen^{1,2}, R. Plume¹, S. J. Gibson¹, A.R. Taylor¹, C. M. Brunt³

ABSTRACT

We have observed ^{12}CO $J = 2 \rightarrow 1$ and $J = 1 \rightarrow 0$, and ^{13}CO $J = 1 \rightarrow 0$ emission in two regions of HI Self-Absorption (HISA) in Perseus: a small, isolated HISA feature called the *globule* and a more extended HISA cloud called the *complex*. Using both Large Velocity Gradient and Monte Carlo radiative transfer codes we found that, in the globule, $N(^{12}\text{CO}) < 6.0 \times 10^{15} \text{ cm}^{-2}$ which, using PDR models, implies that $N(\text{H}_2) < 9.9 \times 10^{20} \text{ cm}^{-2}$. In the complex we found that the H_2 column densities ranged from $1.2 - 2.2 \times 10^{21} \text{ cm}^{-2}$. By comparing the HISA and CO observations we are able to constrain the physical conditions and atomic gas fraction (f). In the globule, $8 \text{ K} < T_{\text{spin}} < 22 \text{ K}$ and $0.02 < f < 0.2$ depending on whether the (unknown) gas density is 10^2 , 10^3 , or 10^4 cm^{-3} . In the complex, $12 \text{ K} < T_{\text{spin}} < 24 \text{ K}$, $0.02 < f < 0.05$, and we were also able to constrain the gas density ($100 < n < 1200 \text{ cm}^{-3}$). These results imply that the gas in the HISA clouds is colder and denser than that usually associated with the atomic ISM and, indeed, is similar to that seen in molecular clouds. The small atomic gas fractions also imply that there is a significant molecular component in these HISA clouds, even when little or no ^{12}CO is detected. The level of ^{12}CO detected and the visual extinction due to dust is consistent with the idea that these HISA clouds are undergoing a transition from the atomic to molecular phase.

Subject headings: ISM: clouds — ISM: globules — ISM: molecules — ISM: structure — submillimeter — radiative transfer

¹Department of Physics and Astronomy, University of Calgary, 2500 University Dr. NW, Calgary, AB, T2N 1N4, Canada

²Currently at Department of Physics & Astronomy, McMaster University, 1280 Main St. W Hamilton, ON, L8S 4M1, Canada

³Department of Astronomy, University of Massachusetts, Amherst, Lederle Graduate Research Tower, MA 01003

1. Introduction

The study of cold ($T < 100$ K) atomic gas, a major component of the interstellar medium in the Galaxy, is a difficult problem. While HI emission lines can be used to easily map the distribution of the atomic gas, it is often difficult to separate the warm and cold components. On the other hand, direct observations of cold HI gas can be obtained from HI lines seen in *absorption* against warm, background HI emission (called HI self-absorption or HISA). Studies of HISA in molecular clouds have shown that the HISA is often well mixed with molecular gas (Jackson et al. 2002, Li & Goldsmith 2003).

Using data from the Canadian Galactic Plane Survey (CGPS; Taylor 1999, Taylor et al. 2003), Gibson et al. (2000; 2005a; 2005b) have revealed HISA in unprecedented detail over a square degree in Perseus. In Gibson et al. (2000; hereafter G2000) two regions in the Perseus arm were found to be of particular interest. The first, labeled the *globule*, is a compact (unresolved in the 1' main beam of the CGPS), dark (absorption line center contrast > 42 K; Gibson et al. 2005b) region with narrow ($\Delta V_{FWHM} = 2.5$ km s $^{-1}$) HISA substructure. IRAS 60 μ m dust continuum emission was observed in the globule, but there was no detected ^{12}CO $J=1\rightarrow 0$ emission (Heyer et al. 1998). The second, labeled the *complex*, is part of a larger HI region. It also shows a deep HISA feature (line center contrast ~ 28 K; Gibson et al. 2005b) and 60 μ m emission. However, unlike the globule, it has detected ^{12}CO $J=1\rightarrow 0$ emission ($T_R^* \approx 1.12$ K; Heyer et al. 1998). Figure 1 shows the general region of study, with both the globule and complex labeled. Unfortunately, while HISA lines can be readily identified throughout the Galaxy, it is difficult to extract physical parameters (density, temperature, column density etc.) from the observations.

Using a new technique, G2000 were able to set limits on mass, temperature, optical depth, density and column density in the globule and the complex. However, the range of these limits was quite large, mainly due to the unknown molecular gas fraction in the two regions. In the globule, no ^{12}CO $J=1\rightarrow 0$ was detected to the limiting sensitivity of the Outer Galaxy Survey of Heyer et al. (1998) (hereafter OGS). In the complex, ^{12}CO $J=1\rightarrow 0$ was detected but, with only one molecular transition, it is difficult to determine the total ^{12}CO column density. Therefore, in this paper, we present observations of ^{12}CO $J=1\rightarrow 0$ and $J=2\rightarrow 1$ in both the globule and the complex in order to determine the molecular gas content. Our goals are to complement the HISA observations presented in G2000, and to better constrain the physical properties of the gas in these two regions.

2. Observations

Our observations of the $J=1 \rightarrow 0$ transition of ^{12}CO ($\nu = 115.3$ GHz) and ^{13}CO ($\nu = 110.2$ GHz) were obtained at the Five Colleges Radio Astronomy Observatory (FCRAO) in 2000 February and May. These ^{12}CO data were obtained in order to either detect the $J=1 \rightarrow 0$ or, at least, achieve a better sensitivity than the OGS data. The ^{13}CO data were obtained to help determine whether the multiple spectral features seen in some of the ^{12}CO observations were due to multiple line-of-sight clouds or self-absorption in the ^{12}CO . The FCRAO 14 m telescope has a full width half maximum (FWHM) beamsize of $45.5''$ at 115 GHz, and main beam efficiency (η_{mb}) of 42%. The velocity resolution (channel width) of these observations is 0.252 km s^{-1} .

The $J=2 \rightarrow 1$ transition of ^{12}CO ($\nu = 230.6$ GHz) was observed at the Caltech Submillimeter Observatory (CSO) in 2001 September. The CSO is a 10.4 m telescope on Mauna Kea, Hawaii, with a FWHM beamsize of $32''$, and η_{mb} of 69% (at 230 GHz). The velocity resolution of these observations was 0.063 km s^{-1} .

In the globule, we observed a single point at the central position in the $J=1 \rightarrow 0$ transition and an 8 point map with full CSO ($32''$) beam spacings in the $J=2 \rightarrow 1$ transition. A ninth position at a half beam spacing ($\Delta\alpha = 0, \Delta\delta = -16''$) was also observed at the CSO. In the complex, we observed a 9 point strip in both ^{12}CO transitions, as well as the $J=1 \rightarrow 0$ transition of ^{13}CO . The strip starts at the central position (labeled as Position 1 in Figure 1), where ^{12}CO $J=1 \rightarrow 0$ emission had been detected in the OGS, and moves outwards at constant Galactic longitude but increasing Galactic latitude (from $b = +0.91^\circ$ to $+0.97^\circ$ in steps of $25''$) to where ^{12}CO $J=1 \rightarrow 0$ had not been previously detected. The spacing of the complex observations were approximately equal to FCRAO half beam spacings. The observed positions in both the globule and the complex are shown in Figure 1.

3. Results

In Sections 3.1 and 3.2 that follow, we first provide details of the observed spectra and then show how the results are used to obtain the molecular gas column densities.

3.1. Description of the Spectra

Figure 2 shows a postage stamp map of the ^{12}CO $J=2 \rightarrow 1$ transition (solid line) and the HISA (dotted line) in the globule, with the single half-beam spaced ($\Delta\delta = -16''$) observation

shown in the middle panel for clarity. Gaussian profiles were fit to the spectra, the parameters of which are listed in Table 1 under the heading *32'' Resolution*. Positions with no detected emission are listed with their 1σ rms noise limits.

To facilitate comparison of the $J=1\rightarrow 0$ and $J=2\rightarrow 1$ transitions, the $J=2\rightarrow 1$ observations were convolved to match the $45''$ beam of the FCRAO. The far right panel in Figure 2 shows the convolved ^{12}CO $J=2\rightarrow 1$ spectrum (solid line) along with the FCRAO $J=1\rightarrow 0$ spectrum (dashed line) at the central position of the globule. The ^{12}CO $J=2\rightarrow 1$ emission is clearly visible in the convolved spectrum, but below the peak-to-peak noise level of the $J=1\rightarrow 0$ observations. This shows that molecular gas is present, but that even our deeper ^{12}CO $J=1\rightarrow 0$ observations did not reach the sensitivity limit required to detect it. A Gaussian profile was fit to the $J=2\rightarrow 1$ transition, the parameters of which are listed in Table 1 under the heading *Convolved to 45'' resolution*. Since there was no signal detected in the $J=1\rightarrow 0$ transition, the 1σ rms noise was used as an upper limit on signal strength.

Figure 2 clearly shows that, while the HISA component of the globule lies at $V_{LSR} = -41 \text{ km s}^{-1}$, the ^{12}CO emission is centered at $V_{LSR} = -45 \text{ km s}^{-1}$. This suggests that these two emission lines are tracing separate clouds along the line of sight. This suggestion is supported by recent observations of the region with an increased signal to noise ratio in the ^{12}CO $J=1\rightarrow 0$ transition (Brunt, 2005) which reveal a number of weak ^{12}CO knots in the vicinity of the globule at a V_{LSR} of -45 km s^{-1} . To draw comparisons with the atomic globule at $V_{LSR} \approx -41 \text{ km s}^{-1}$ we use the 1σ rms noise limit for both the $J=1\rightarrow 0$ and $J=2\rightarrow 1$ transitions ($T_{mb} = 0.58$ and 0.06 K respectively) as an upper limit on line strength. As an approximation to a line width, we use the FWHM of the HISA lines ($\Delta V_{FWHM} = 2.5 \text{ km s}^{-1}$). This is a valid assumption if the atomic and molecular gas components are mixed and the line widths are dominated by turbulence. This assumption is supported by the similarities between the HISA and ^{12}CO line widths seen in the complex. These line parameters are used in Section 3.2.1 to constrain the molecular gas content of the globule.

The bottom half of each panel in Figure 3 shows the HISA as a function of position in the complex. The top halves show the ^{12}CO $J=2\rightarrow 1$ (solid line), ^{12}CO $J=1\rightarrow 0$ (dashed line), and ^{13}CO $J=1\rightarrow 0$ (dotted line) at the same positions. Note that Figure 3 is a single strip of observations (of increasing Galactic latitude) and is only presented as what appears to be a nine point map for readability. Figure 3 shows interesting changes in the spectral line profiles progressing from the cloud core (Position 1) to the edge (Position 9). The first two positions show emission peaks at $\sim -40 \text{ km s}^{-1}$ with blueshifted shoulders (or secondary peaks) at $\sim -41 \text{ km s}^{-1}$. The third position is singly peaked, while the fourth through sixth positions have emission peaks at -41 km s^{-1} with *redshifted* shoulders (or secondary peaks) at -40 km s^{-1} . The emission drops off rapidly after Position 6, with Positions 7 through 9

showing no significant signal. ^{13}CO and ^{12}CO observations show similar line profiles, which is suggestive of emission from multiple clouds (as opposed to self absorption). We will test this assumption in the next section. Gaussian profiles were fit to the spectra in the complex and are listed in Table 2. Note that Positions 1 and 2 were fit with 2 separate Gaussians.

Figure 4 shows the result of smoothing the ^{12}CO $J=2\rightarrow 1$ in the complex to the velocity resolution of the HI observations (solid lines of ^{12}CO $J=2\rightarrow 1$ are overlayed on the dotted HISA profiles). This spectral resampling blends the multiple ^{12}CO components (seen best in Positions 1 and 2) into one component. While there is general agreement between the HISA and the smoothed ^{12}CO emission lines, the profiles do not match exactly. This could be due to a number of different factors: a greater spatial extent for the HISA than for the ^{12}CO , different beamsizes of the observations, or errors in the background subtraction of the HISA features. Positions 7 through 9 are not shown due to the lack of molecular emission at those positions.

3.2. Molecular Gas Column Densities

There are a number of techniques for solving the equations of radiative transfer and detailed balance in molecular clouds. However, to determine the physical parameters of the molecular components of the globule and the complex, we used a Large Velocity Gradient (LVG; i.e. Goldsmith et al. 1983) model which offers a rudimentary approach to determining the bulk properties of a region based on the integrated intensities of the observed lines. These models employed the collision rates of Flower & Launay (1985) and Shinke et al. (1985).

In this section, we describe the method by which we determined the molecular gas column densities from our CO observations. The results of this analysis will be used in Section 4 to constrain the physical properties of the HISA clouds, as well as the atomic gas fraction.

3.2.1. The Globule

To determine the molecular gas content in the HISA globule itself, we are interested in ^{12}CO emission at $V_{LSR} = -41 \text{ km s}^{-1}$. However, since there is no detectable signal at this velocity we set an upper limit to the ^{12}CO column density by using the 1σ rms noise of the ^{12}CO $J=2\rightarrow 1$ transition ($T_{mb} = 0.06 \text{ K}$). In lieu of any actual CO detection in the globule, we used a range of parameters chosen to cover the likely range of physical conditions. Thus, for the globule, we used kinetic temperatures from 8 K to 50 K and fixed the density at

10^2 , 10^3 , and 10^4 cm $^{-3}$ to check for differences between sub-thermal and LTE excitation of the ^{12}CO lines. For each temperature-density combination, we used our LVG code to calculate the ^{12}CO $J=2\rightarrow 1$ brightness for a series of 50 different column densities. The column densities ranged from $5 \times 10^{14} - 5 \times 10^{17}$ cm $^{-2}$ and were logarithmically-spaced. Thus, by comparing our 1σ noise limit to the LVG models, we were able to set an upper limit to the ^{12}CO column density for each temperature-density combination. The maximum ^{12}CO column density, corresponding to the lowest temperature-density combination (8K and 100 cm $^{-3}$ respectively), is 9.5×10^{15} cm $^{-2}$.

At such small column densities, ^{12}CO self-shielding is very inefficient and the $\text{H}_2/^{12}\text{CO}$ abundance ratios can be strongly affected. However, using the photodissociation region (PDR) models of van Dishoeck & Black (1988), and assuming that the strength of the UV field is that of the average interstellar radiation field (i.e. $G_o = 1$), we can estimate the total H_2 column density in the globule. For our maximum ^{12}CO column density of 9.5×10^{15} cm $^{-2}$, the van Dishoeck & Black curves provide an H_2 column density of $N(\text{H}_2) < 1.1 \times 10^{21}$ cm $^{-2}$.

3.2.2. The Complex

For the complex, we only modeled the spectrally smoothed data since they are most directly comparable to the HISA spectra. In our models we used kinetic temperatures of 12 K to 50 K (at temperatures lower than 12K we were unable to find a LVG fits to our ^{12}CO data). At each temperature we created a 50×50 logarithmically-spaced grid of LVG models in density-column density parameter space. The densities ranged from $10^2 - 5 \times 10^4$ cm $^{-3}$, and the ^{12}CO column densities from $5 \times 10^{15} - 5 \times 10^{18}$ cm $^{-2}$. The observed line intensities were fit to the grid of LVG models using a χ^2 minimization routine to find the density–column density combination that best fit the observations at each temperature. Again, comparing our ^{12}CO column densities to the models of van Dishoeck & Black (1988), we also determined the H_2 column densities. The results of this LVG analysis will be presented in Section 4.1.

To test our assumption that the multiple velocity components seen in the complex were due to separate clouds rather than self-absorption in a single cloud, we also ran an extensive series of Accelerated Monte Carlo (AMC; Hogerheijde & van der Tak, 2000) models. AMC models have the advantages of producing model spectra based on the input physical parameters of the cloud (i.e. temperature, density and velocity gradient), and a greater available range of parameter space. While LVG models incorporate the simplifying assumption that the concentric model shells are radiatively decoupled, this is not the case for the more robust AMC models.

We first attempted to model the cloud as a single entity with a variety of density, temperature, abundance, and velocity gradients. Some models, in which the abundance ratio was varied with a power law on the order of 0.5 came close to matching the ^{12}CO spectra, but no single model (for any position) was able to match the ^{12}CO and ^{13}CO line profiles and ratios, despite attempts at varying the $^{12}\text{CO}/^{13}\text{CO}$ abundance ratio. In addition, none of these models were capable of matching the shift in the red-blue asymmetry discussed previously. In all, we ran several thousand models. The total parameter space covered is shown in Table 3. Column 1 shows the parameters that were varied and column 2 shows the range of central values used for each parameter. Models were run as powerlaw functions of the form $x(r) = x_o \left(\frac{r_o}{r}\right)^\alpha$ where x_o is the value of the parameter (abundance, temperature, density) at some characteristic radius (r_o), α is the power law index, and r is the radius. α was allowed to vary between -2 and +2, except for variations in the density for which $\alpha > 0$ would be unphysical. We also tried modeling each individual position as a separate and distinct “cloudlet”, with its own unique temperature, density and velocity gradients. Again, none of the models were able to reproduce the spectra across the entire complex. Therefore, we are reasonably confident that the multiple velocity components seen in the spectra are due to separate line of sight clouds.

4. Discussion

4.1. Atomic and Molecular Gas Components in HISA Clouds

Gibson et al. (2000) presented a preliminary view of HISA features seen in the CGPS, finding a number of small scale HISA features that had not previously been seen in single-dish surveys. In more recent papers (Gibson et al. 2005a & 2005b) present a much more detailed view of HISA features through a re-analysis of the CGPS data, using automated algorithms to locate HISA features in the HI data cube instead of the “by-eye” identification used in the earlier paper. In addition, Gibson et al (2005b) contains a revision of the HISA data presented in G2000. In the earlier paper the HISA amplitudes were in error; the correct HISA amplitudes are lower than those listed in G2000. In this section we use these improved HISA observations and the technique presented in Gibson et al. (2000) to determine the physical properties of HISA gas.

The technique presented by G2000 allows one to constrain the physical properties of the HISA gas in the complex and the globule by placing limits on the optical depth and spin temperature of the HISA features. The optical depth of the HISA can be determined through:

$$\tau_{HISA} = \frac{CN_{tot}f}{T_K \Delta v} \quad (1)$$

Where C is combination of constants for the HI spin-flip transition = 5.2×10^{-19} (Dickey & Lockman 1990), Δv is the line width, T_K is the kinetic temperature of the gas which, under the assumptions of G2000 should be the same as T_s , the HI spin temperature, and N_{tot} is the *total* column density (i.e. $N_{atomic} + N_{molecular}$).

This analysis was able to find families of solutions based upon allowed ranges of the unknown atomic gas fraction ($f = N(HI)/[N(HI) + N(H_2)]$) and p , the fraction of HI emission originating behind the HISA cloud. Figure 6 of G2000 shows their results. Even if we make the reasonable assumption that p is close to unity, indicating that most of the cold HI is in the foreground as would be needed for strong HI self-absorption, the unknown atomic gas fraction still limits our ability to determine the amount and temperature of the HISA gas. For example, Figure 6 of G2000 shows that in the complex, if the HISA is warm ($T_k > 40$ K) then $f \sim 1$ and the HISA opacity (τ_{HISA}) is approximately 1 to 2, whereas if the HISA is cold ($T_k < 10$ K) then $f < 0.1$ and τ_{HISA} is constrained to $\sim 0.4 - 0.5$.

With our LVG analysis of the ^{12}CO observations, we are able to better constrain the HISA properties (f , T , and τ) in the globule and complex, by finding the overlap between the original parameter space of G2000 and the parameter space defined by our ^{12}CO observations. For the HISA gas, this was done according to the procedure detailed in G2000 but using the corrected data as given in Gibson et al. 2005b. For our ^{12}CO observations, we took the derived H_2 column density for each position (Section 3.2) and, using the above equation, calculated τ_{HISA} for a range of atomic gas fractions (f) from 0.01 to 1.

Figure 5 shows an example for the Globule in which we plot τ_{HISA} vs T_{spin} . For this figure we have assumed that $n(H_2) = 10^2 \text{ cm}^{-3}$ in our LVG calculation. The dotted curves show the values of p , the thin, tilted strips (starting at the upper-left corner of the plot) show τ_{HISA} vs T_{spin} as determined from the Gibson et al. (2000) analysis of the HISA features for a range of assumed atomic gas fraction (f), and the wider, tilted strips (starting in the bottom-right corner of the plot) show τ_{HISA} vs T_{spin} as determined from our ^{12}CO analysis for a range of atomic gas fractions. The bold “sharkfin”-shaped region shows the union of the HISA and ^{12}CO solutions for all values of f , where each individual intersection is for a particular f only. As can be seen from Figure 5, the inclusion of the ^{12}CO data significantly constrains the allowed range of physical conditions in the HISA gas. The “sharkfin” corresponds to a solution of $8 \text{ K} < T_{spin} < 11 \text{ K}$ and $0.5 < \tau_{HISA} < 5.8$. If we make the further assumption that $p > 0.8$ (i.e. that most of the HI emission is in the background as would be required to produce strong HISA features), then $0.5 < \tau_{HISA} < 0.8$.

In addition, since the intersection of HISA and ^{12}CO solution also corresponds to an intersection of f , we can constrain the atomic gas fraction, and find that $f = 0.02 - 0.06$. A similar analysis was done for assumed densities of 10^2 and 10^3 cm^{-3} in the globule, and for each position in the complex. The results are given in Table 4. Note that no solutions were found for the Complex - Positions 1 & 2. This is probably due to the presence of the strong second spectral feature. Since the LVG analysis was done on the spectrally smoothed data (to match the spectral resolution of the HISA observations) the two line-of-sight clouds are treated as a single component (see Figure 4). The atomic gas fraction in Positions 3 through 6 were found to be $f = 0.02 - 0.1$. The combination of the HISA and molecular observations also allow us to better constrain the molecular gas density and column density since we now have a better constraint on the kinetic temperature. The results are given in Table 5.

Given the small atomic gas fractions, the complex and the globule seem to be predominantly molecular in composition. While this seems obvious for the central positions in the complex where the ^{12}CO lines are relatively strong, it is less obvious for Position 6, where the ^{12}CO lines are weak. Nevertheless our analysis suggests that $> 90\%$ of the gas is molecular. It is even more puzzling in the globule where the ^{12}CO lines are undetectable and yet our limits on the ^{12}CO column density suggest that up to 95% to 98% of the gas could be molecular. Thus it is possible that the globule and the edge of the complex are regions where the gas has a large molecular component that is not well-traced by ^{12}CO . There are, however, possible alternative explanations. Gibson et al (2000) derived the spin temperature of the HISA features via the equation

$$T_s = \sqrt{\frac{\langle P \rangle f_n C \Delta s}{k \tau_o \Delta V}} \quad (2)$$

Two main assumptions that go into producing equation (2) are: a) the volume density is equal to the column density divided by the path length through the cloud (Δs) and, b) the volume density is related to the spin temperature through the ideal gas law. Therefore, if either the gas pressure $\langle P \rangle$ is below the canonical value of $P/k = 4000 \text{ K cm}^{-3}$, or the HISA features are thinner along the line-of-sight than assumed by G2000, then the atomic gas fraction would have to be larger than predicted to produce the same spin temperature. However, to produce gas which is primarily atomic (i.e. $f \sim 1$) would require either a large drop in gas pressure or significantly foreshortened clouds. While there is no evidence to support the hypothesis of significantly lower than average gas pressures, there is evidence to support the notion that observationally identified clouds may be preferentially *elongated* along the line of sight rather than foreshortened (e.g. Heiles 1997) due to observational selection effects.

We can estimate the total mass contained in the 45" beam of our FCRAO ^{12}CO $J = 1 \rightarrow 2$ observations from the solutions given above and using a distance to Perseus of 2 kpc. The upper limit for the total gas mass in the globule ($M(\text{HI}) + M(\text{H}_2)$) is $1.3 - 3M_\odot$ for the given range of temperatures, H_2 column densities, and atomic gas fractions. This range is between 7 and 60 times lower than the Jeans masses calculated for the globule for the given ranges of temperature and density. A similar calculation for the complex finds that each 45" beam contains $3 - 4M_\odot$ of material. This is again 7 to 60 times lower than the Jeans mass implying that neither the globule nor the individual positions in the complex are gravitationally bound.

4.2. The Nature of the HISA Clouds

So what are these HISA clouds? They appear to be non-gravitationally bound regions of cold, primarily molecular, gas that is not detected in ^{12}CO . Such regions are not unusual in high-latitude cirrus clouds and have been traced via excess IR emission (e.g. Heiles, Reach, & Koo 1988; Reach, Koo & Heiles 1994). However, most of the cirrus clouds in which ^{12}CO does not seem to trace the total amount of molecular gas are relatively warm ($T_K > 30\text{K}$), low density ($n(\text{H}_2) < 100 \text{ cm}^{-3}$) regions in which the HI does not appear to be self absorbed. In contrast, the temperatures (10 K - 25 K) and densities ($n(\text{H}_2) \sim 100 - 1200 \text{ cm}^{-3}$) in our HISA clouds are similar to those seen in molecular clouds. Thus, the HISA gas has temperatures and densities that bridge the gap between the ambient atomic ISM and the colder, denser molecular medium.

Could these HISA clouds be sites where atomic gas is condensing into the molecular phase required for star formation? Although critical to the evolution of matter in the Galaxy, molecular condensation is poorly understood. Using a model that assumes that molecular clouds form from atomic gas after the passage of shock waves, Bergin et al. (2004) find that the molecular cloud formation timescale is not controlled by the formation rate of H_2 on grains but, rather, by the shielding of molecules from the UV radiation. While the H_2 can self-shield quite efficiently, ^{12}CO formation requires shielding of the interstellar radiation by dust grains. If the total A_V is greater than ~ 0.7 then there is enough material present to effectively shield the ^{12}CO .

Using the 60 and 100 μm IRAS HIRES data, we have estimated the dust temperature and the amount of visual extinction in the globule and at each of our observed positions in the complex. Following the procedure outlined in Wood et al. (1994), we calculated the dust temperature from the ratio of the 60 and 100 μm fluxes, assuming that the dust is optically thin, that the 60 and 100 μm beam solid angles are roughly equivalent, and that

the dust emissivity spectral index is 1.5. We find that the dust temperatures are all $< 30\text{K}$. If the dust is optically thin, knowing the temperature allows us to determine the $100\text{ }\mu\text{m}$ dust opacity from the ratio of the observed $100\text{ }\mu\text{m}$ flux to the Planck function. The dust visual extinction was then calculated from the relationship between A_V and the $100\text{ }\mu\text{m}$ dust opacity provided by Wood et al. (1994), which is a functional fit to the data given in Jarrett et al. (1989). In the complex, the dust visual extinction ranges from $A_V = 3.8$ at Position 1 to $A_V = 2.2$ at Position 6. For Positions 7 through 9, A_V drops below 2, as it does in the globule where $A_V = 1.2$. Note that these are the visual extinctions through the *entire* cloud. The edge-to-center visual extinctions, which are directly comparable to the Bergin et al. (2004) models, are half these values. Thus, these results are consistent with the scenario given by Bergin et al (2004) in which the absence of detectable ^{12}CO in the globule, and in Positions 7 - 9 of the complex, is due to the limited UV shielding provided by the dust in these regions. However, there could still be a considerable amount of molecular gas in Positions 7 - 9 and in the globule, since H_2 can form at considerably earlier times and lower column densities than ^{12}CO .

Since A_V in the globule and at the edge of the complex is close to the critical value needed to shield ^{12}CO from the interstellar radiation field, it is possible that these regions are in the process of forming ^{12}CO . Thus, over time, ^{12}CO lines may eventually become observable as the ^{12}CO abundance continues to increase. Bergin et al. (2004) predict the observed intensities of various transitions as a function of time (as clouds evolve from atomic to molecular). In their model, a cloud with a $^{12}\text{CO } J = 2 \rightarrow 1$ line strength less than 0.06 K (our 1σ detection limit) would be less than 10^7 years old. This “age” is consistent with the minimum transit time between spiral arms in the outer Galaxy ($\sim 10^7$ years; Heyer & Tereby 1998).

An alternative scenario is that instead of being molecular clouds in the process of formation, the HISA clouds could represent transient events, or even the dispersal of molecular clouds into the atomic medium. While we cannot rule out these possibilities, the formation scenario seems more likely since the Complex and the Globule both seem to be correlated with a region slightly downstream of the spiral shock wave in the Perseus arm (Gibson et al 2005; Roberts 1972) where the gas is densest. This is precisely the type of region where we would expect H_2 to be condensing from HI .

5. Conclusions

Using $^{12}\text{CO } J = 2 \rightarrow 1$ observations from the CSO, and ^{12}CO and $^{13}\text{CO } J = 1 \rightarrow 0$ observations from the FCRAO, we have determined the molecular gas content in two regions

of HI Self-Absorption (HISA) in Perseus. In the globule we observed a small 8-point map at the CSO to match the $45''$ resolution, single-point $J = 1 \rightarrow 0$ observation taken with the FCRAO. In the complex we observed a nine point strip from the center of the cloud to the edge of the cloud in increasing galactic latitude. No ^{12}CO $J = 2 \rightarrow 1$ emission was detected in the globule to a 1σ rms limit of 0.06 K. ^{12}CO was detected in Positions 1 through 7 in the complex but fell below the 1σ rms noise limit in Position 8 and 9. Positions 1 & 2 were found to contain two spectral features which we determined to be due to separate line-of-sight clouds rather than to ^{12}CO self absorption.

Using both Large Velocity Gradient and Monte Carlo radiative transfer codes, we were able to determine the molecular gas content in the globule and complex. In the globule $N(^{12}\text{CO}) < 6.0 \times 10^{15} \text{ cm}^{-2}$, implying that $N(\text{H}_2) < 9.9 \times 10^{20} \text{ cm}^{-2}$. In the complex we found that the H_2 column densities ranged from $1.2 - 2.2 \times 10^{21} \text{ cm}^{-2}$.

By comparing the HISA and ^{12}CO observations we are able to constrain the physical conditions and atomic gas fraction (f) of these two regions. In the globule, $8 \text{ K} < T_{\text{spin}} < 22 \text{ K}$ and $0.02 < f < 0.2$ depending on whether the (unknown) gas density is 10^2 , 10^3 , or 10^4 cm^{-3} . In the complex, $12 \text{ K} < T_{\text{spin}} < 24 \text{ K}$, $0.02 < f < 0.05$, and the gas density is constrained ($100 < n < 1200 \text{ cm}^{-3}$). These results imply that the gas in the HISA clouds is colder and denser than that usually associated with the atomic ISM and, indeed, is similar to that seen in molecular clouds. The small atomic gas fractions also imply that there is a significant molecular component in HISA clouds, even when little or no ^{12}CO is detected. The level of ^{12}CO detected and the visual extinction due to dust is consistent with the idea that these HISA clouds are undergoing a transition from the atomic to molecular phase.

The authors would like to thank Floris van der Tak for his help with the Monte Carlo Models, and the Natural Sciences and Engineering Research Council of Canada for their financial support. The Five College Radio Astronomy Observatory is operated with the permission of the Metropolitan District Commission, Commonwealth of Massachusetts, and with the support of the National Science Foundation under grant AST 01-00793. The CSO is funded under a grant from the National Science Foundation.

REFERENCES

Bergin, E. A., Hartmann, L. W., Raymond, J. C., & Ballesteros-Paredes, J. 2004, *ApJ*, 612, 921

Brunt, C. M. 2005, in prep.

Dickey, J. M., & Lockman, F.J. 1990, *ARA&A*, 28, 215

Evans, N. J., Rawlings, J. M. C., Shirley, Y. L., & Mundy, L. G. 2001, *ApJ*, 557, 193

Flower, D.R., & Launay, J.M. 1985, *MNRAS*, 214, 217

Gibson, S.J., Taylor, A.R., Higgs, L.A., & Dwedney, P.E. 2000, *ApJ*, 540, 851

Gibson, S.J., Taylor, A.R., Higgs, L.A., Brunt, C. M., & Dwedney, P.E. 2005a, *ApJ*, in press

Gibson, S.J., Taylor, A.R., Higgs, L.A., Brunt, C. M., & Dwedney, P.E. 2005b, *ApJ*, in press

Goldsmith, P.F., Young, J.S., & Langer, W.D. 1983, *ApJS*, 51, 203

Heiles, C. 1997, *ApJ*, 481, 193

Heiles, C., Reach, W. T., & Koo, B. 1988, *ApJ*, 332, 313

Heyer, M. H., & Tereby, S. 1998, *ApJ*, 502, 265

Heyer, M. H., Brunt, C.M., Snell, R.J., Howe, J.E., Schloerb, F.P., & Carpenter, J.M. 1998, *ApJS*, 115, 241

Hogerheijde, M.R., & van der Tak, F.F.S. 2000, *A&A*, 362, 697

Jackson, J. M., Bania, T. M., Simon, R, Kolpak, M, Clemens, D. P., & Heyer, M. H. 2002, *ApJ*, 566, L81

Jarrett, T. H., Dickman, R. L., & Herbst, W. 1989, *ApJ*, 345, 881

Li, D., & Goldsmith, P. F. 2003, *ApJ*, 585, 823

Reach, W. T., Koo, B-C., & Heiles, C. 1994, *ApJ*, 429, 672

Roberts, W. W. Jr. 1972, *ApJ*, 173, 259

Schinke, R., Engel, V, Buck, U, Meyer, H, & Diercksen, G.H.F. 1985, *ApJ*, 299, 939

Taylor A. R., 1999, in *ASP Conf. Proc 168* (San Francisco; ASP), pg 3

Taylor, A.R., Gibson, S.J., Peracaula, M, Martin, R.G., Landecker, T.L., Brunt, C.M., Dewdney, P.E., Dougherty, S.M., Gray, A.D., Higgs, L.A., Kerton, C.R., Knee, L.B.G., Purton, C.R., Uyaniker, B, Wallace, B.J., & Willis, A.G. 2003, AJ, 125, 3145

van Dishoeck, E.F., & Black, J.H. 1988, ApJ, 334, 771

Wood, D. O. S., Myers, P. C., & Daugherty, D. A. 1994, ApJS, 95, 457

Table 1: ^{12}CO Gaussian Fits in the Globule

| J=1→0 transition | | | | J=2→1 transition | | | |
|---------------------------------|----------------------------|-----------------|------------------------------|-------------------------|-----------------|------------------------------|-------------------------|
| $\Delta\alpha$ ($''$) | $\Delta\delta$ ($''$) | T_{mb} (K) | V_{LSR} (km s $^{-1}$) | FWHM (km s $^{-1}$) | T_{mb} (K) | V_{LSR} (km s $^{-1}$) | FWHM (km s $^{-1}$) |
| 32 $''$ Resolution | | | | | | | |
| 0 | 0 | - | - | - | 0.33 | -45.1 | 1.13 |
| 0 | -64 | - | - | - | <0.14 | - | - |
| +32 | -32 | - | - | - | <0.20 | - | - |
| +32 | 0 | - | - | - | <0.13 | - | - |
| 0 | +32 | - | - | - | <0.07 | - | - |
| -32 | 0 | - | - | - | <0.13 | - | - |
| -32 | -32 | - | - | - | <0.12 | - | - |
| 0 | -32 | - | - | - | 0.52 | -45.1 | 1.5 |
| 0 | -16 | - | - | - | 0.54 | -45.0 | 1.21 |
| Convolved to 45 $''$ Resolution | | | | | | | |
| 0 | 0 | <0.58 | - | - | 0.35 | -45.0 | 1.2 |

Table 2: ^{12}CO Gaussian Fits in the Complex

| Position | J=1→0 transition | | | | | J=2→1 transition | | |
|----------|----------------------------|----------------------------|-----------------|------------------------------|-------------------------|--------------------|------------------------------|-------------------------|
| | $\Delta\alpha$ ($''$) | $\Delta\delta$ ($''$) | T_{mb} (K) | V_{LSR} (km s $^{-1}$) | FWHM (km s $^{-1}$) | T_{mb} (K) | V_{LSR} (km s $^{-1}$) | FWHM (km s $^{-1}$) |
| | 45 $''$ Resolution | | | | | 32 $''$ Resolution | | |
| 1 | 0 | 0 | 2.7 | -41.4 | 1.2 | 2.4 | -41.7 | 1.3 |
| ... | ... | ... | 9.5 | -39.8 | 1.0 | 6.4 | -39.7 | 1.5 |
| 2 | +12.9 $''$ | +22.5 $''$ | 7.1 | -41.4 | 1.4 | 3.1 | -41.6 | 1.5 |
| ... | ... | ... | 8.5 | -39.8 | 1.3 | 5.7 | -39.8 | 1.4 |
| 3 | +25.8 $''$ | +45.0 $''$ | 8.3 | -40.8 | 2.6 | 6.3 | -40.7 | 2.3 |
| 4 | +38.8 $''$ | +67.8 $''$ | 8.3 | -41.0 | 2.2 | 5.8 | -41.0 | 2.2 |
| 5 | +51.6 $''$ | +90.3 $''$ | 7.6 | -41.0 | 2.0 | 4.6 | -41.1 | 2.0 |
| 6 | +64.5 $''$ | +112.8 $''$ | 3.6 | -41.1 | 2.4 | 1.3 | -41.1 | 2.1 |
| 7 | +77.4 $''$ | +135.3 $''$ | <0.22 | - | - | <0.08 | - | - |
| 8 | +90.5 $''$ | +158.1 $''$ | <0.19 | - | - | <0.07 | - | - |
| 9 | +103.4 $''$ | +180.6 $''$ | <0.25 | - | - | <0.06 | - | - |

Table 3: AMC Model Parameters for the Complex.

| Parameter | Range |
|---|--|
| Kinetic Temperature | 10 - 70 K |
| Volume Density | 100 - 6000 cm ⁻³ |
| ¹² CO/H ₂ Abundance Ratio | 10 ⁻⁴ - 10 ⁻⁷ |
| Radial Velocity | 0 - 3 km s ⁻¹ |
| Turbulent Linewidth | 0.05 - 1 km s ⁻¹ |
| Cloud Radius | 10 ¹⁵ - 10 ¹⁹ cm |

Table 4: Range of Physical Conditions in HISA Clouds (assuming $p > 0.8$)

| Position | T_{spin} (min) | T_{spin} (max) | τ_{HISA} (min) | τ_{HISA} (max) |
|--|------------------|------------------|---------------------|---------------------|
| Complex - Position 1 | | | no solution | |
| Complex - Position 2 | | | no solution | |
| Complex - Position 3 | 14.5 | 23.7 | 0.4 | 0.5 |
| Complex - Position 4 | 14.5 | 22.4 | 0.3 | 0.6 |
| Complex - Position 5 | 13.9 | 20.0 | 0.4 | 0.6 |
| Complex - Position 6 | 12.0 | 18.0 | 0.4 | 0.5 |
| Globule ($n = 10^2 \text{ cm}^{-3}$) | 8.0 | 11.0 | 0.5 | 0.8 |
| Globule ($n = 10^3 \text{ cm}^{-3}$) | 10.0 | 20.2 | 0.6 | 0.9 |
| Globule ($n = 10^4 \text{ cm}^{-3}$) | 11.0 | 22.1 | 0.6 | 0.9 |

Table 5: Molecular Gas Properties

| Position | J = 1 → 0 | | J = 2 → 1 | | n(H ₂) cm ⁻³ | N(¹² CO) cm ⁻² | N(H ₂) K | T _K cm ⁻² |
|----------------------|----------------------|--|----------------------|--|--|--|-------------------------|------------------------------------|
| | T _{mb} K | ΔV _{FWHM} km s ⁻¹ | T _{mb} K | ΔV _{FWHM} km s ⁻¹ | | | | |
| Complex - Position 1 | 8.6 ^a | 1.3 | 5.0 | 2.6 | 120 | 3.2×10 ¹⁷ | 2.2 × 10 ²¹ | 20 ^b |
| Complex - Position 2 | 8.0 ^a | 2.9 | 4.6 | 2.7 | 370 | 1.2×10 ¹⁷ | 1.8 × 10 ²¹ | 20 ^b |
| Complex - Position 3 | 8.2 ^a | 2.6 | 6.1 | 2.4 | 2220 | 3.2×10 ¹⁶ | 1.3 × 10 ²¹ | 20 |
| Complex - Position 4 | 8.0 ^a | 2.3 | 5.7 | 2.3 | 1840 | 2.9×10 ¹⁶ | 1.2 × 10 ²¹ | 20 |
| Complex - Position 5 | 7.3 ^a | 2.1 | 4.5 | 2.1 | 1150 | 4.3×10 ¹⁶ | 1.3 × 10 ²¹ | 15 |
| Complex - Position 6 | 3.6 ^a | 2.5 | 1.3 | 2.1 | 140 | 5.7×10 ¹⁶ | 1.5 × 10 ²¹ | 15 |
| Globule | < 0.58 | - | < 0.06 | - | 100 | < 6.0 × 10 ¹⁵ | 9.9 × 10 ²⁰ | 10 |
| Globule | < 0.58 | - | < 0.06 | - | 10 ³ | < 4.0 × 10 ¹⁴ | 5.3 × 10 ²⁰ | 15 |
| Globule | < 0.58 | - | < 0.06 | - | 10 ⁴ | < 1.0 × 10 ¹⁴ | 4.2 × 10 ²⁰ | 15 |

^a - Spectral line properties from the spectrally smoothed data.

^b - Assumed temperature based on HISA-CO analysis in Positions 3 - 6 (Table 4).

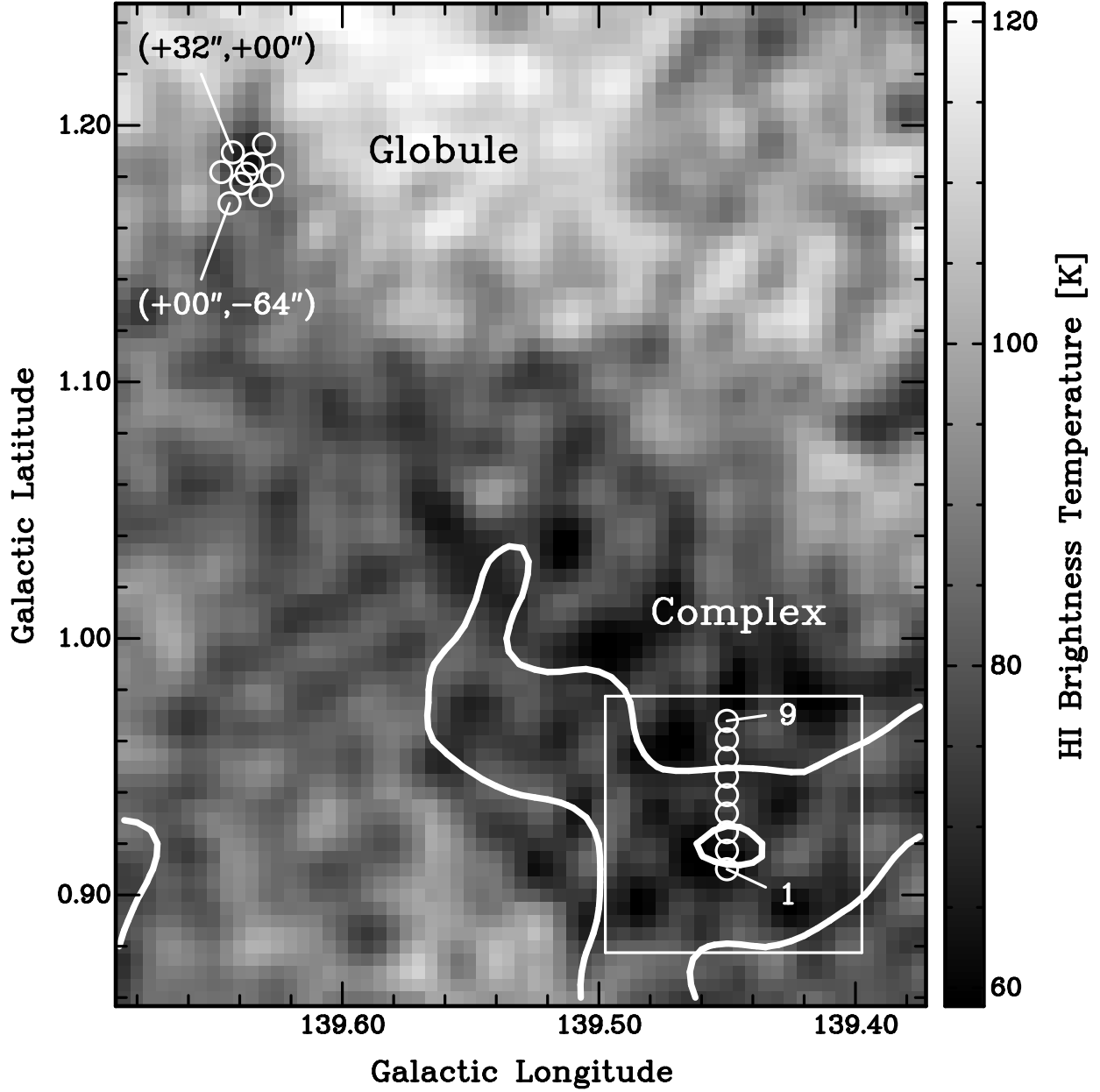


Fig. 1.— **Region of study:** The complex and globule, as defined by Gibson et al. (2000). The grayscale background is the HI brightness and the contours denote the ^{12}CO $J = 1 \rightarrow 0$ brightness at 1 and 3 K (from Heyer et al. 1998). The positions which were mapped are labeled in the inset image. The central coordinates of the *globule* are: $\ell \sim 139.635^\circ$, $b \sim +1.185^\circ$ or $\alpha(J2000) = 3^h09^m24.0^s$, $\delta(J2000) = +59^\circ30'22.5''$. The central coordinates of the *complex* (labeled as Position 1) are $\ell \sim 139.45^\circ$, $b \sim +0.91^\circ$ or $\alpha(J2000) = 3^h07^m3.5^s$, $\delta(J2000) = +59^\circ21'38.5''$.

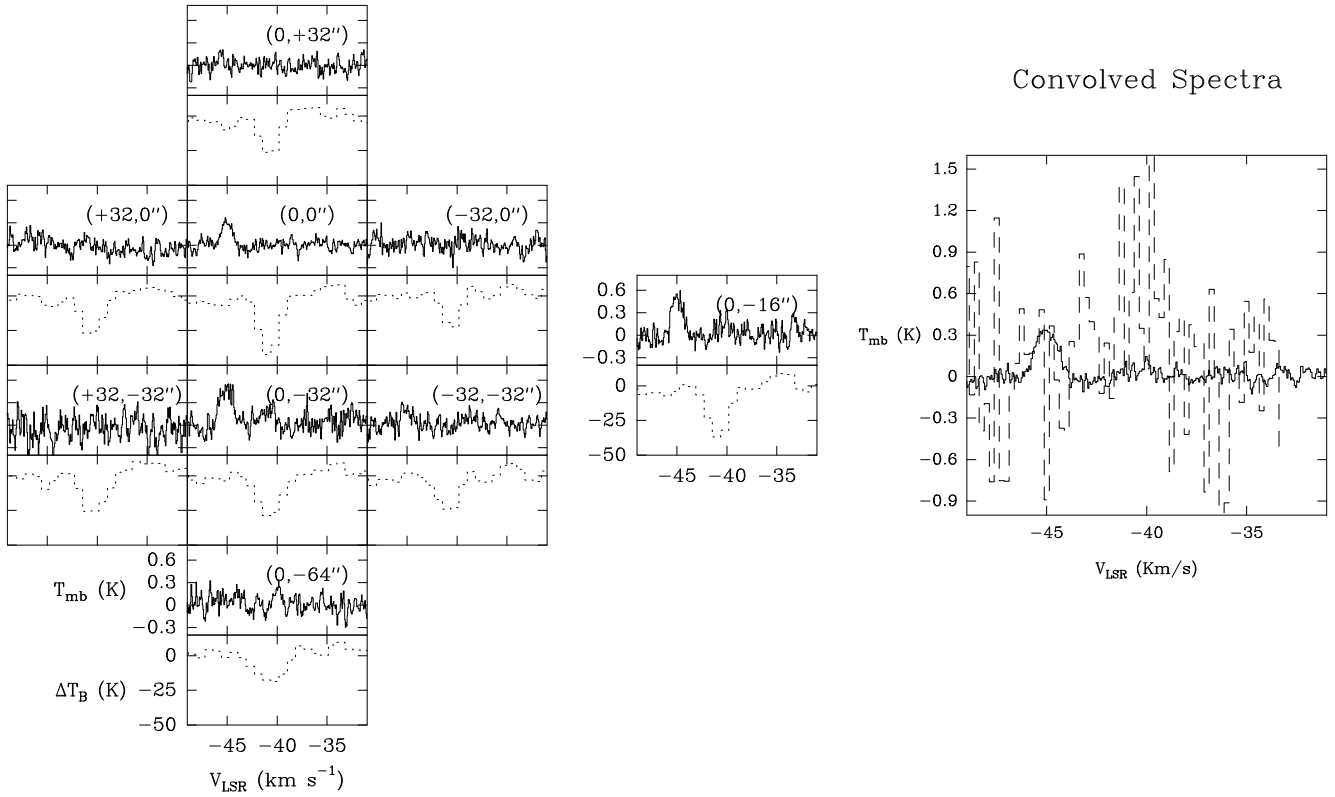


Fig. 2.— **Left Panel:** $J=2\rightarrow 1$ map of the globule taken at the CSO with a $32''$ beam. Note that the half beam spacing observation has been offset (to the right) for clarity. The top portion of each position shows the $J=2\rightarrow 1$ transition of ^{12}CO (solid line), while the bottom portion shows the HISA at that position (dotted line). **Middle Panel:** Same as above but shows the single half-beam spaced observation in the globule (see text). **Right Panel:** Superposition of the ^{12}CO $J=2\rightarrow 1$ CSO observations convolved to the FCRAO $45''$ beam (solid lines) and $J=1\rightarrow 0$ FCRAO observations (dotted lines) of the globule.

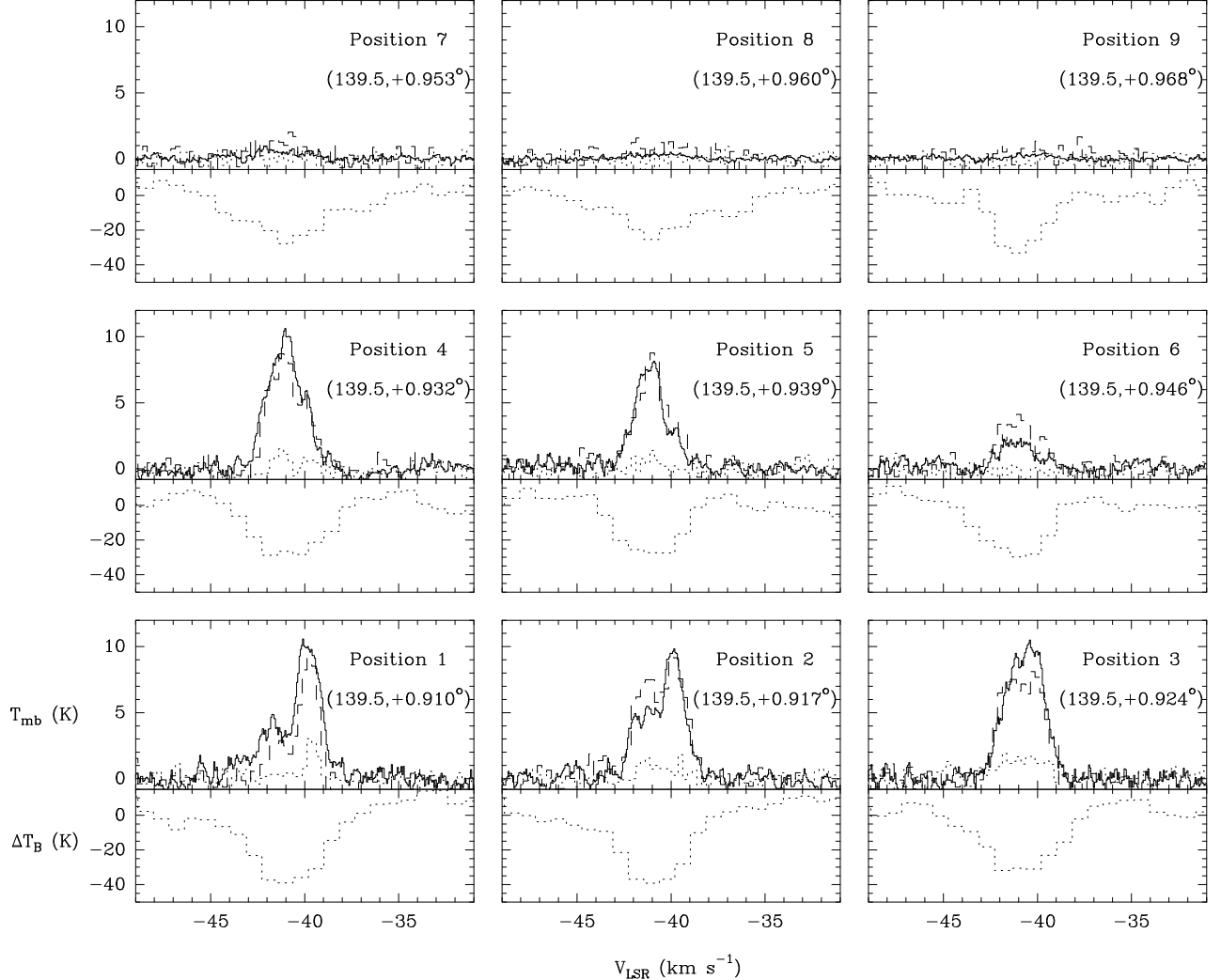


Fig. 3.— Individual spectra for each position in the complex (labeled 1 through 9). The bottom panel of each position shows the HISA profile, while the top panel shows the ^{12}CO $J=2-1$ (solid), $J=1-0$ (dashed) and ^{13}CO $J=1-0$ (dotted) profiles at the position. The Galactic longitude and latitude are given in the parentheses in each panel (in degrees).

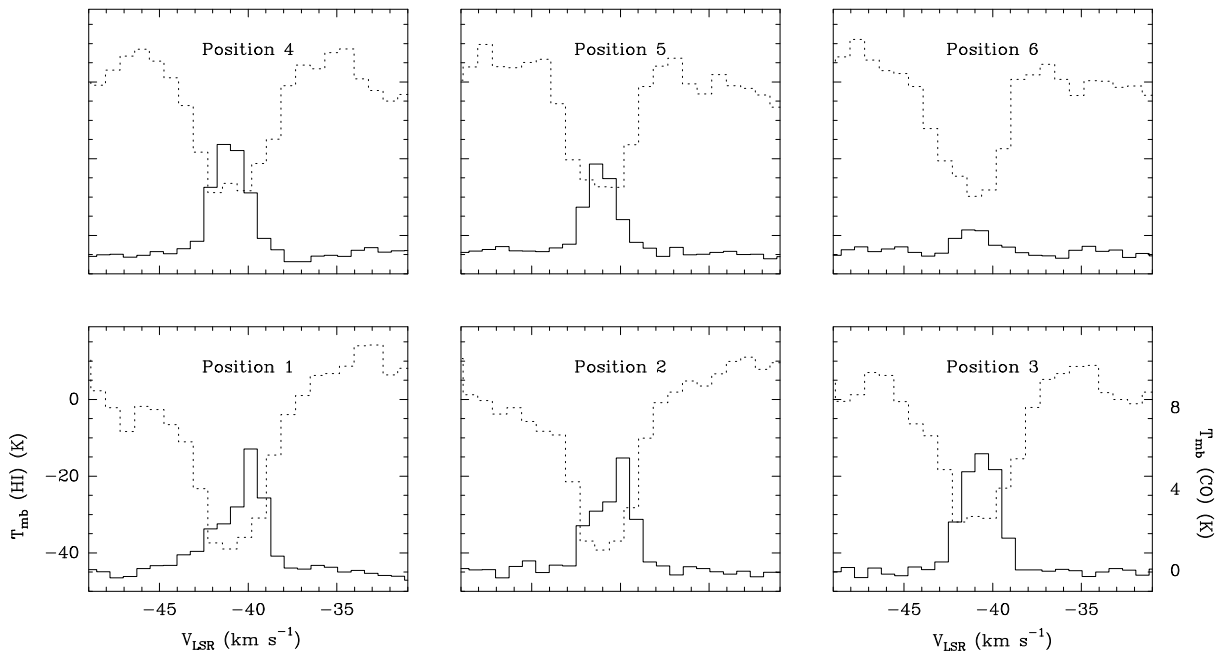


Fig. 4.— ^{12}CO $J=2\rightarrow 1$ Observations (solid line) in the complex smoothed to the same velocity resolution as the HISIA observations (dashed lines).

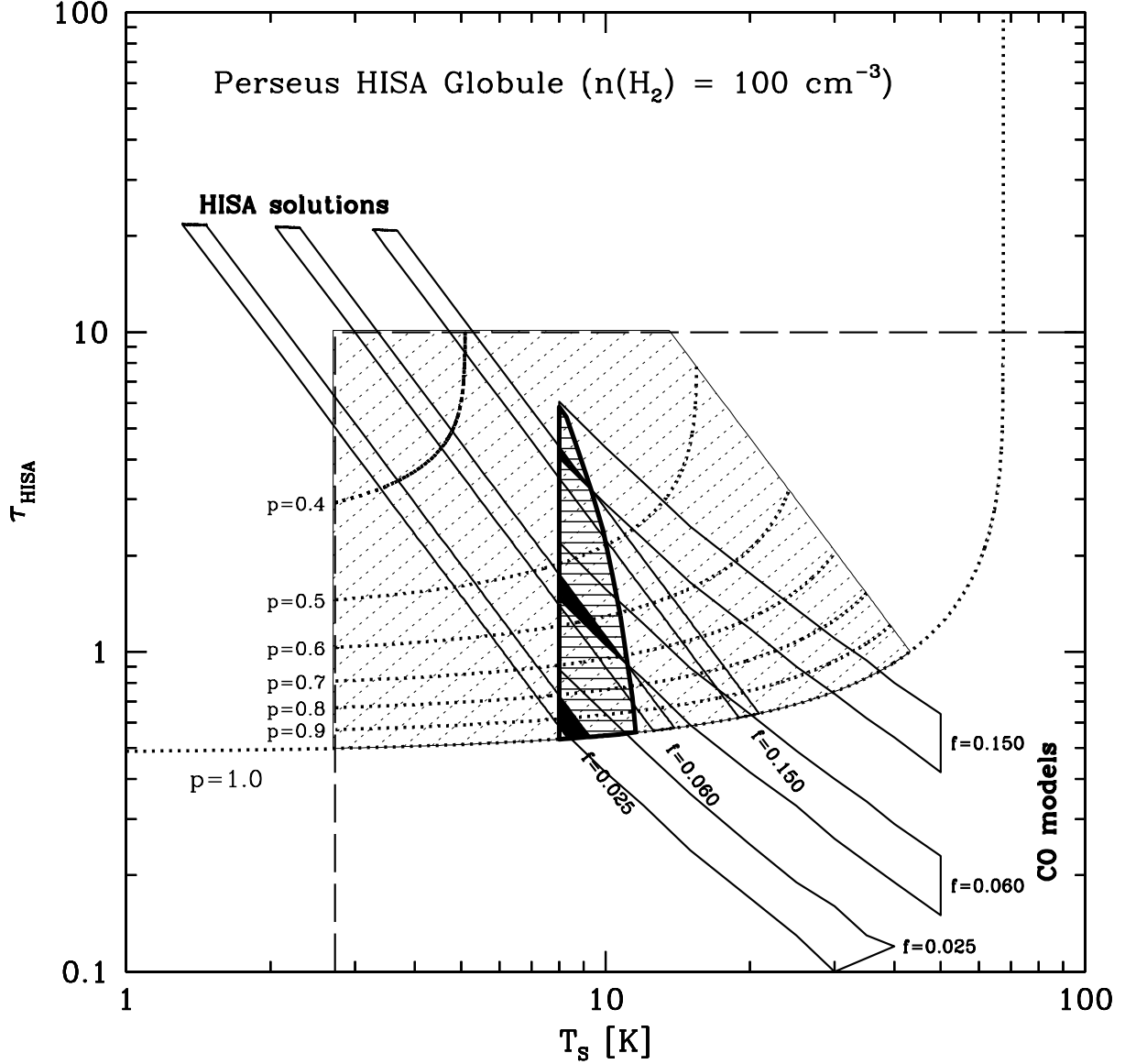


Fig. 5.— Physical parameters of the HISA gas in the globule as derived by atomic and molecular observations. The lightly shaded area shows the parameter space determined from the original HISA analysis presented in G2000. The dotted curves show the values of p , the thin, tilted strips (starting at the upper-left corner of the plot) shows τ_{HISA} vs T_{spin} as determined from the Gibson et al. (2000) analysis of the HISA features for a range of assumed atomic gas fraction (f) , and the wider, tilted strips (starting in the bottom-right corner of the plot) shows τ_{HISA} vs T_{spin} as determined from our ^{12}CO analysis for a range of atomic gas fractions. The bold “sharkfin”-shaped region shows the union of the HISA and ^{12}CO solutions for all values of f , where each individual intersection is for a particular f only.